Electrochemical Synthesis of CdSe and CdSe/ZnO Films: Morphological, Structural and Electronic Properties

Gökmen SIĞIRCIK[*1] **ORCID** *0000-0002-5457-8372*
Tunç TÜKEN[1] **ORCID** *0000-0002-0559-2848*

[1]*Çukurova University, Faculty of Science and Letters, Chemistry Department, Adana*

Abstract

CdSe films were electrochemically prepared on ITO electrode in aqueous solution applying a constant potential. Structural, morphological and optical features of CdSe thin films were examined with FE-SEM, XRD and UV-visible spectrophotometry techniques. XRD results revealed CdSe films were deposited, in the form of cubic crystals from aqueous solution of Cd^{2+} and Se^{4+}, in presence of Na_2SO_4 supporting electrolyte. Band gap values of CdSe films were found between 1.88 and 2.0 eV. Wide band gap ZnO was electrochemically deposited on narrow band gap CdSe to improve its optoelectronic properties. Band gap value of CdSe/ZnO nanonorods was determined as 2.7 eV. Mott-Schottky equation was utilized to calculate flat band potential (E_{FB}), as well as charge carrier density (N_D) of materials. N_D values were found as 1.623×10^{20} and 9.186×10^{20} cm^{-3} for CdSe and CdSe/ZnO, respectively. ZnO offers higher stability and lower band gap is promising material to be utilized in solar cell applications.

Keywords: CdSe/ZnO, Semiconductor materials, Electrochemical deposition

CdSe ve CdSe/ZnO Filmlerin Elektrokimyasal Sentezi: Morfolojik, Yapısal ve Elektronik Özellikler

Öz

CdSe filmler ITO elektrot üzerinde sabit potansiyel uygulayarak sulu çözeltide elektrokimyasal yolla hazırlanmıştır. CdSe ince filmlerin yapısal, morfolojik ve optik özellikleri FE-SEM, XRD ve UV-görünür spektrofotometri teknikleri çalışılmıştır. XRD sonuçları, CdSe filmlerin Na_2SO_4 destek elektroliti varlığında Cd^{2+} ve Se^{4+} içeren sulu çözeltiden kübik kristal formda biriktirildiği görülmüştür. CdSe filmlerin bant aralığı değerleri 1,88 ve 2,0 eV aralığında bulunmuştur. Geniş bant aralığına sahip ZnO dar bant aralığına sahip CdSe üzerine optoelektronik özelliklerini geliştirmek için elektrokimyasal yolla biriktirilmiştir. CdSe/ZnO nanoçubukların bant aralığı değeri 2,7 eV olarak belirlenmiştir. Mott-Schottky eşitliği malzemelerin düz bant potansiyelini (E_{FB}) ve yük taşıyıcı yoğunluğunu (N_D) hesaplamak için

---

[*]Corresponding author (Sorumlu yazar): Gökmen SIĞIRCIK, *gsigircik@cu.edu.tr*

kullanılmıştır. N_D değerleri, CdSe ve CdSe/ZnO için 1.623×10^{20} ve 9.186×10^{20} cm^{-3} olarak bulunmuştur. Daha yüksek kararlılık ve düşük bant aralığı sağlayan ZnO, güneş pili uygulamalarında kullanılmak için umut verici bir malzemedir.

Anahtar Kelimeler: CdSe/ZnO, Yarıiletken malzemeler, Elektrokimyasal biriktirme

1. INTRODUCTION

The ability to meet increasing energy request and environmental concerns gradually increase the interest in alternative energy production techniques [1,2]. Hydrogen has much higher energy conversion efficiency as a fuel than other commonly utilized energy sources. Furthermore, its environmentally friendly and sustainable feature has also increased the interest in hydrogen-based fuel cells. There are various methods for hydrogen production using solar energy. Among them, photo electrochemical splitting of water into oxygen and hydrogen molecules is considered to be the most promising and inexpensive method [3,4]. While photo electrochemical cells provide a low-cost, easy-to-apply, environmentally friendly solution, there is still a need for further improvement in efficiency/cost ratio. In photo electrochemical cells, n or p-type semiconductor materials that comprise significant physical and optical properties are used as photo electrode. Thus, good absorption ability, chemical stability and low cost in the solar spectrum are the anticipated properties of the semiconductor materials [5]. Therefore, there is a great effort to develop semiconductor materials used in environmentally friendly fuel production applications by splitting of water using solar energy. The improvements that can be made increase the photo catalytic efficiency of the semiconductor electrode materials [6]. Opto-electronic property of semiconductors, which is directly dependent on its morphological and crystallographic properties, is extremely important for the device applications. Besides, it is well known that the synthesis parameters and method have a direct influence on morphological and opto-electronic features of semiconductor materials [7]. Semiconductors have wide band gap; such as ZnO, TiO_2 and SnO_2 or narrow band gap semiconductors like CdSe, CdTe, and CuO are the most utilized materials for this purpose [8].

II-VI group semiconductor materials have been utilized for a long time owing to their various application areas; for instance electronic, light emitting/detecting devices and photovoltaic solar cells [9]. Among them, CdSe is a significant material for electronic devices and photo electrochemical solar cells. Energy band gap for CdSe, an n-type semiconductor, is around 1.74 eV [10]. CdSe is used in thin film transistors, photo electrochemical solar cells, photo conductors and γ-ray detectors because of its high photo sensitivity in visible area. CdSe are also preferred due to their properties such as high efficiency radiation recombination and absorption coefficient, direct band transition and quantum size effect. The size dependent property of CdSe nanostructures has a significant effect on band gap energy. This situation greatly affects physical properties of the material that are important for potential applications [11,12]. CdSe has two different crystal structures, including cubic and hexagonal [12,13]. Moreover, the photo response of a narrow band gap semiconductor lengthens more into range of visible wavelength than a wide band gap semiconductor. However, due to rapid recombination rate of photo generated electron/hole (e/h^+) pairs, a narrow band gap semiconductor offers lower photo catalytic efficiency [14]. There is requirement to enhance optical and electronic behavior of a narrow band gap semiconductor for different applications. Therefore, many efforts have been applied to improve their opto-electronic properties. One of them is combination of a narrow band gap semiconductor and a wide band gap semiconductor [15]. This provides more effective charge separation and higher transport rate of e/h^+ pairs [16].

Among II-VI oxide semiconductor compounds, ZnO is the most used material with hexagonal wurtzite structure, as well as wide band gap value

(3.37 eV) [17]. ZnO nanostructures have attracted much interest by researchers due to its remarkable electrical, optical and mechanical characteristics [18]. For this reason, it has been frequently pronounced as strong candidate for various purposes like light emitting diodes, dye-sensitized solar cells, gas sensor and photo-catalysts [19-22]. Moreover, the feasibility of ZnO is strictly affected by its morphological and crystallographic properties for these applications [23]. 1D metal oxide semiconductors (like nanofiber, nanotube and nanorod) have been extensively used. Rod-like ZnO nanostructures offer straight pathway for transportation of photo generated electrons that recombination rate decreases through the bulk material [24].

In present study, CdSe films were deposited on ITO electrode via electrochemical technique at different deposition time, in aqueous solution. First of all, the optimal electro synthesis parameters were determined by using CV technique. Rod-like ZnO was deposited electrochemically on CdSe to enhance its opto-electronic properties. N_D values were found as 1.623×10^{20} and 9.186×10^{20} cm^{-3} for CdSe and CdSe/ZnO, respectively with help of Mott-Schottky equation.

2. MATERIALS AND METHOD

2.1. Materials

Indium tin oxide (ITO) electrode (8-12 Ω cm^{-2}) was used. Moreover, cadmium sulphate 8/3 hydrate (CdSO$_4$.8/3H$_2$O), selenium dioxide (SeO$_2$), potassium chloride (KCl), zinc nitrate tetra hydrate (Zn(NO$_3$)$_2$.4H$_2$O), sodium sulphate (Na$_2$SO$_4$), sodium hydroxide (NaOH), ethanol (C$_2$H$_5$OH), sulphuric acid (H$_2$SO$_4$) materials were utilized without purification.

2.2. Electrochemical Deposition of CdSe Thin Films

Electrochemical deposition of CdSe nanomaterials was done in three-electrode system at 80±2 °C in water bath. ITO electrodes were utilized as working electrode for electrochemical deposition of CdSe. Reference electrode and counter electrode were Ag/AgCl (3 M KCl) and platinum sheet, respectively. Firstly, ITO electrodes were ultrasonically cleared by using sodium hydroxide solution, ethanol and distilled water for 5 minutes, respectively. Cycling voltammetry (CV) technique was carried out at 10 mV s^{-1} scan rate for ITO electrode in different deposition solutions. The deposition solution was a consisted of 0.01 M CdSO$_4$ + 0.001 M SeO$_2$ + 0.1 M Na$_2$SO$_4$. pH value of solutions was arranged to 2.5 by diluted H$_2$SO$_4$ solution. The deposition of CdSe nanostructures was done at -0.70 V constant potential employing diverse deposition times between 3 and 20 minutes. After electrochemical deposition process, CdSe nanomaterials were cleaned by distilled water and finally dried at room temperature.

2.3. Electrochemical Deposition of ZnO Nanorods on CdSe

Electrochemical synthesis of ZnO nanomaterials was applied in three-electrode system. Temperature of deposition solutions was held at 70±2 °C by using water bath. For electrochemical deposition of ZnO nanostructures, ITO/CdSe electrode where CdSe thin film was deposited at 3 minutes deposition time was the working electrode. In addition, Ag/AgCl (3 M KCl) was used as reference electrode and platinum sheet was the counter electrode. Deposition solution was comprised 0.01 M Zn(NO$_3$)$_2$ and 0.1 M KCl. Electrosynthesis of ZnO was employed at current value of -0.30 mA cm^{-2} for 30 minutes deposition time. After electrochemical deposition process, CdSe/ZnO nanomaterials were cleaned with distilled water and finally dried under room temperature.

2.4. Characterization of CdSe and CdSe/ZnO Nanorods

The surface morphology of CdSe materials was examined via field emission scanning electron microscopy (FE-SEM, Zeiss, Supra 55). Elemental composition of CdSe nanomaterials was determined with FE-SEM equipped by energy dispersive X-ray spectroscopy (EDX). Besides, X-ray diffraction (XRD, Rigaku, SmartLab) was used to study crystallographic features of CdSe

nanostructures. The optical behavior of semiconductor nanomaterials was investigated via UV-visible Spectrophotometer (Perkin Elmer, Lambda 25).

2.5. Electrochemical Measurements

Mott-Schottky measurement was utilized by electrochemical impedance spectroscopy method. For this technique, 5 mV amplitude was the applied at 1000 Hz frequency in 0.1 M Na_2SO_4 solution.

3. RESULTS AND DISCUSSION

3.1. The CV Results of ITO

The CV technique was realized to determine the appropriate electrochemical parameters for synthesis of CdSe on ITO electrode surface. The CV measurement was obtained from 0.0 to -1.0 V in 0.1 M Na_2SO_4 (pH= 2.5) at 10 mV s^{-1} scan rate, given in Figure 1a. While significant change was not observed in the current over a wide potential range, a slight increase in current started from around -0.6 V. This situation is associated with the reduction reactions of hydrogen ions and In_2O_3/SnO_2 species. However, the ITO electrode appears to be electrochemically stable in wide potential range in this solution.
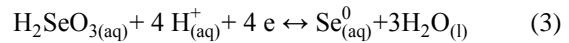
The CV obtained in 0.01 M $CdSO_4$ and 0.1 M Na_2SO_4 (pH= 2.5) was given in Figure 1b. There was not any noticeable current change indicating to Faradaic process, in a wide potential range. Once electrode potential arrived at -0.70 V, during scan, reduction of Cd^{2+} ions gave raise cathodic current increase. Moreover, the oxidation of freshly reduced metallic Cd was observed as anodic current increase, during the backward scan, again starting at -0.70 V. The relevant equations for reversible equilibrium of Cd^{2+}/Cd are given as below [25]:

$$Cd_{(aq)}^{2+}+ 2e \leftrightarrow Cd_{(s)} \qquad (1)$$
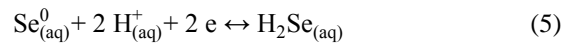
$$E=-0,403+0,0295 \log (Cd^{2+}) \qquad (2)$$

From equation 2, theoretically, the reversible electrode potential value is calculated as -0.68 V, for Cd^{2+}/Cd equilibrium. It is apparent that there is quite small overvoltage for the onset of this electrochemical reaction.

The CV studies were also realized in presence of 0.001 M SeO_2 with 0.1 M Na_2SO_4 (pH= 2.5), in Figure 1c, at which Na_2SO_4 was again the supporting electrolyte. The reduction of Se^{4+} could start at around -0.40 V, however further reduction steps could also take place beyond -0.70 V. The observed first cathodic peak is related to reduction of Se^{4+} to Se^0, between the potentials -0.40 V and -0.70 V. The further reduction process is explained with equation 5. During the backward scan, the anodic peak appeared at around -0.30 V, which corresponds to oxidation of species on the surface. These species are the product of reduction reactions occurred at the previous forward scan [26].

$$H_2SeO_{3(aq)}+ 4 H_{(aq)}^+ + 4 e \leftrightarrow Se_{(aq)}^0 +3H_2O_{(l)} \qquad (3)$$

$$E=0,741-0,059 \, pH+0,0148 \log (H_2SeO_3) \qquad (4)$$

$$Se_{(aq)}^0+ 2 H_{(aq)}^+ + 2 e \leftrightarrow H_2Se_{(aq)} \qquad (5)$$

$$E=-0,399-0,059 \, pH-0,0295 \log (H_2Se) \qquad (6)$$

In Figure 2a, the CV result of the ITO electrode obtained in 0.01 M $CdSO_4$, 0.001 M SeO_2 and 0.1 M Na_2SO_4 (pH= 2.5) solution was presented. In this case, the reduction of Se^{4+} started at around -0.40 V, and then the reduction of the cadmium ions started and changed the pattern, as well as the current values. Moreover, at backward scan, the anodic peak indicated much higher anodic current (charge) with respect to solely Se^{4+} including electrolyte solution. This was an evidence for the onset of reduction reactions for Se^{4+} and Cd^{2+} consecutively, on ITO surface. For the rest of backward scan, anodic oxidation of Se^{2-} species to Se^0 was observed at around -0.20 V and an extra oxidation peak at around +0.80 V. The later anodic peak is attributed to oxidation of Se^0 type to Se^{4+} ion [27]. In solution containing both Cd^{2+} and Se^{4+}, it was apparent that reduction/oxidation products

alter the ITO surface, thus the electrode/solution interface. This was due to experimental conditions, at which a whole scan is employed in a wide potential range and various types of species (CdSe, metallic Cd, Se^0, Se^{2-}, etc.). The adsorbed species on the surface may create some kind of poisoning effect and/or extra overvoltage, rescheduling the electrochemical reactions.
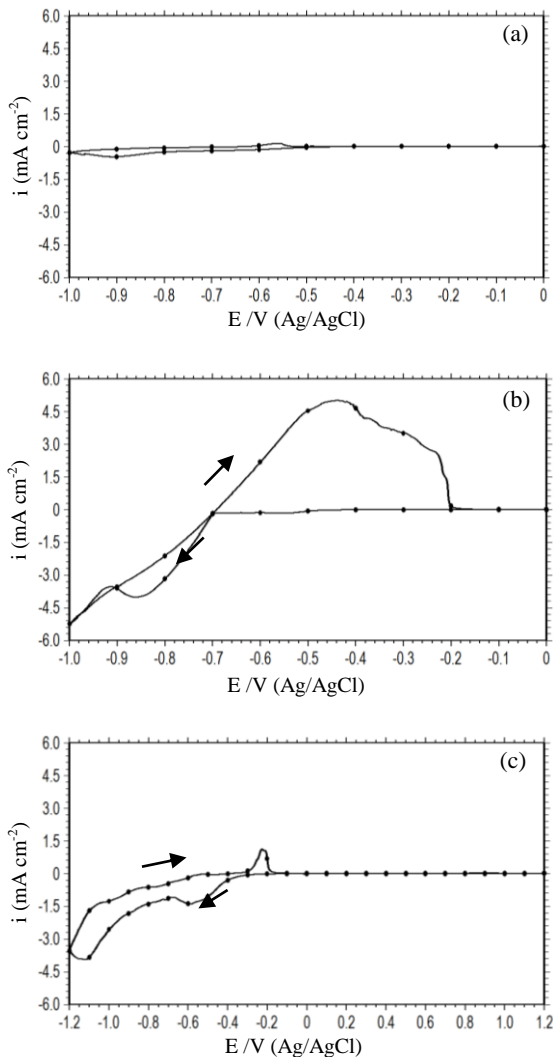
3.2. Electrochemical Deposition of CdSe on ITO

From evaluation of voltammetry results, it was determined that -0.70 V was chosen as the most appropriate potential value for deposition of CdSe compound on ITO surface, since this value is the limit for avoiding bulk deposition of metallic Cd and suitable for production of sufficient Se^{2-} at the interface, offering precise control for deposition of freshly produced Se^{2-} and Cd^{2+} on the surface. Figure 2b shows the chronoamperogram recorded during CdSe deposition in 0.01 M $CdSO_4$, 0.001 M SeO_2 and 0.1 M Na_2SO_4 (pH=2.5) solution, under -0.70 V. Within the first 40 seconds, the nucleation of CdSe nanoparticles happened on the surface of electrode, thus current density values changed remarkably. Afterwards, almost a constant current value was observed, which indicated to consistent deposition process took place on the surface, homogeneously.
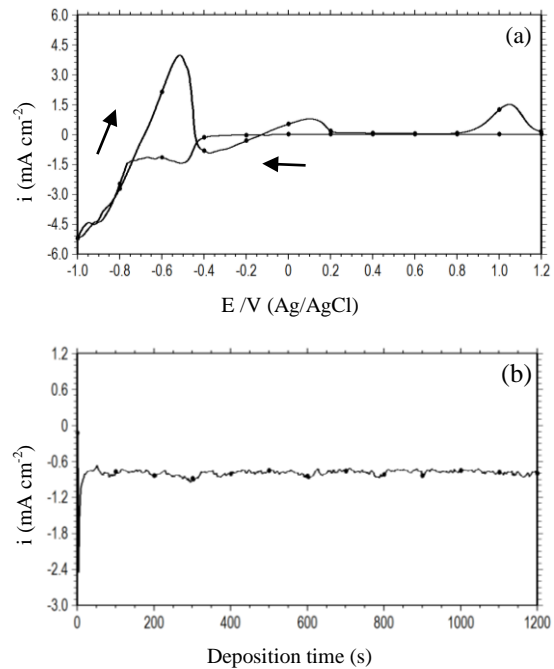

Figure 1. CV result of ITO obtained in 0.1 M Na_2SO_4 solution (a), 0.1 M Na_2SO_4 + 0.01 M $CdSO_4$ solution (b) and 0.1 M Na_2SO_4 + 0.001 M SeO_2 solution (c) with 10 mV/s scan rate

Figure 2. CV result of ITO obtained in 0.01 M $CdSO_4$ + 0.001 M SeO_2 + 0.1 M Na_2SO_4 solution with 10 mV/s scan rate (a) and the chronoamperometry plot during the deposition of CdSe nanostructures at -0.70 V (b)

3.3. Surface Morphology of CdSe Thin Films

FE-SEM images of CdSe nanomaterials obtained at increased deposition times on ITO electrode surface were given in Figure 3. The well-defined and homogenous CdSe nanoparticles with compact form were obtained as clearly seen from FE-SEM images. On the other hand, surface morphology of CdSe films prepared at 3, 5 and 10 minutes were almost similar appearance. Moreover, the number and size of CdSe nanoparticles increased with increasing deposition time. When FE-SEM images of CdSe nanostructures obtained at 15 and 20 minutes deposition period were examined, it was seen that the general morphology did not change significantly, but the particle size increased gradually. Particularly, the particle sizes of CdSe nanoparticles synthesized at 20 minutes deposition period were quite large and distinct. Furthermore, the EDX analysis results of the CdSe nanoparticles prepared in different deposition period were summarized in Table 1. CdSe thin films were electrochemically synthesized almost in the ratio of 1:1 (by atomic %), apart from film deposited at 20 minutes in Table 1. This situation is attributed to higher amount of the selenium ions existing at ITO/solution interface, rather than cadmium ions which should be transported from bulk solution.

Table 1. The elemental ratio of Cd and Se in CdSe nanostructures at different deposition times

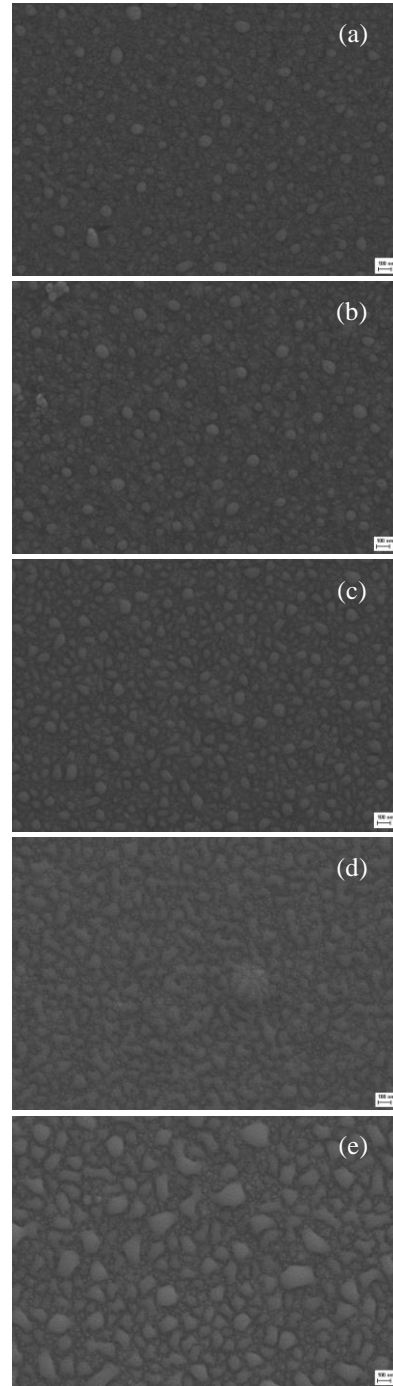| Deposition time (minute)	Cd:Se (atomic ratio %)
3	51.22:48.78
5	52.87:47.13
10	50.60:49.40
15	52.86:47.14
20	40.39:59.61

Figure 3. FESEM images of CdSe nanostructures obtained at different deposition times; 3 (a), 5 (b), 10 (c), 15 (d) and 20 minutes (e)

3.4. Structural Analysis of CdSe Thin Films

XRD analysis was employed to examine the crystallographic properties of electrochemically prepared CdSe films. XRD patterns were given in Figure 4. This result showed that CdSe was obtained in cubic crystal structure. Furthermore, major characteristic peaks were observed at ~25 and ~42° values, for (111) and (220) planes of CdSe, respectively. The achieved results were consistent with literature (PDF card no: 19-0191) [28]. Intensities of observed two peaks were very close to each other for samples prepared with 3 and 5 minutes deposition periods. On the other hand, intensity of the (111) plane peak increased significantly with increasing deposition time. This situation showed that CdSe nanoparticles prepared at 15 and 20 minutes deposition times developed along the dominant (111) plane. As a result, XRD results depicted that CdSe nanomaterials were deposited in the form of cubic crystals.

The crystallite size (D) values of the obtained nanomaterials were calculated as described by Scherrer (Equation 7) [29]. λ and k are the X-ray wavelength (1.54 Å) and a constant (0.9), respectively. θ and β are Bragg diffraction angle and full width at half maximum of material.

$$D = \frac{k\lambda}{\beta\cos\theta} \tag{7}$$

The values of lattice constant (a=b=c), as well as unit cell volume (V) were calculated with the equations 8 and 9 [30]. (hkl) is the Miller indices of lattice constant and d is interplanar spacing of atomic planes.

$$\frac{1}{d_{hkl}^2} = \frac{h^2 + k^2 + l^2}{a^2} \tag{8}$$

$$V = a^3 \tag{9}$$

From evaluation of data summarized in Table 2, it was proved that electrochemically deposited CdSe films have the expected crystal properties from regular CdSe cubic crystals. It was also noticed that the lattice constant values decreased with increasing deposition time and approached the standard value. The determined lattice parameters are consistent with the standard values. The crystallite size values of CdSe nanostructures were calculated in a range of around 4.5 and 6.5 nm. These findings were evidence for deposition of CdSe nanomaterials on ITO surface, by means of -0.70 V (vs. Ag/AgCl) constant potential value, from aqueous solution of Cd^{2+} and Se^{4+}, in presence of Na_2SO_4 supporting electrolyte.
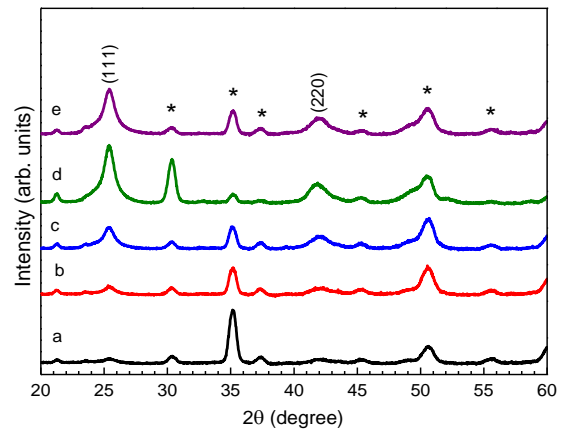

Figure 4. XRD patterns of CdSe nanostructures obtained at different deposition times; 3 (a), 5 (b), 10 (c), 15 (d) and 20 minutes (e) (*: ITO peaks)

Table 2. Structural parameters of CdSe nanostructures obtained from XRD results

Deposition time (minute)	2θ (°)		Lattice parameters (Å)	V (Å³)	Average D values (nm)
	(111)	(220)	a=b=c		
3	25.31	41.77	6.0899	225.86	5.4296
5	25.33	42.21	6.0864	225.47	4.5186
10	25.34	41.93	6.0862	225.44	6.1886
15	25.31	41.67	6.0913	226.01	4.6746
20	25.43	41.99	6.0718	223.85	6.5275

3.5. Optical Properties of CdSe Thin Films

The band gap energy (E_g) value is the critical parameter for semiconductor materials, in aspect of light harvesting efficiency. For this purpose, the E_g values were calculated with help of Tauc equation, plotting $(\alpha h\nu)^2$ versus $h\nu$ [31].

$$\alpha h\nu = A\left(h\nu - E_g\right)^n \qquad (10)$$

In this equation, n and A are direct band transition (n=½) and constant, while plot is extrapolated. The value of n=½ was used since CdSe are direct band gap type semiconductor [32], and the results were given in Figure 5 for electrochemically prepared CdSe films on ITO surface. It was noted that as the deposition time increases, the band gap value decreased gradually. The band gap value of CdSe nanoparticles obtained at 3 and 20 minutes deposition periods decreased from 2.0 to 1.88 eV, respectively.

Band gap energy values of electrochemically prepared CdSe nanomaterials were found to be slightly higher, with respect to previously reported values for bulk CdSe (1.74 eV) [33]. This situation was attributed to quantum size effect phenomena [34], since we have proved that electrochemically produced CdSe nanoparticles have a diameter less than 10 nm (Table 2). Moreover, as obviously seen band gap energy values of CdSe thin films synthesized at 3 and 5 minutes deposition times were not significantly different and this difference decreased considerably with increasing deposition time. Generally, decrease in particle size results in increasing band gap energy of the material, which is known as "blue shift". Thus, absorption at lower wavelengths in the absorption spectrum is observed [11].
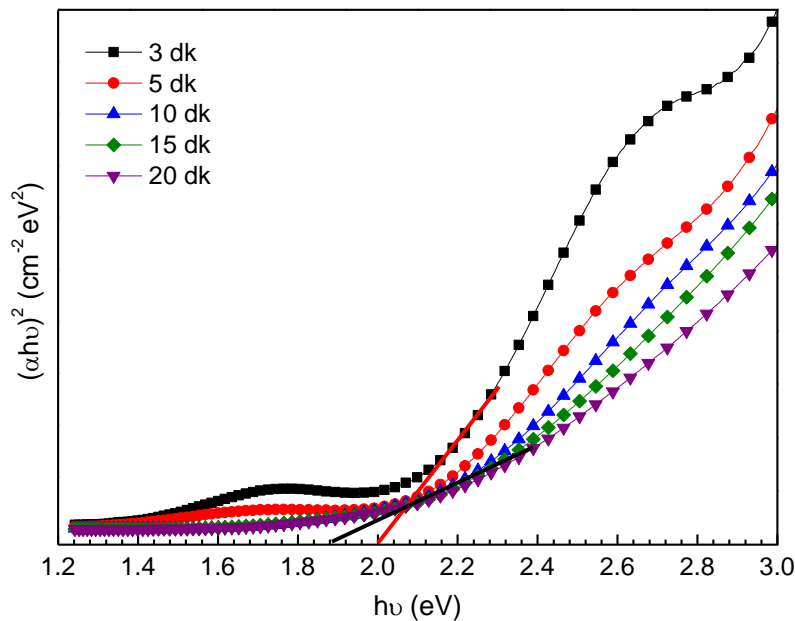

Figure 5. Tauc plots of CdSe nanostructures obtained at different deposition times
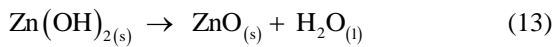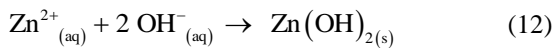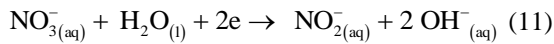
3.6. Electrochemical Deposition of ZnO Nanorods on CdSe

CdSe coated ITO samples were prepared with employing -0.70 V (vs. Ag/AgCl) constant potential value for 3 min deposition time, as described above. Then, the nanorod structured ZnO thin film was deposited galvanostatically, on ITO/CdSe surface. The chronopotentiogram obtained during ZnO synthesis was given in Figure

6a, where the solution composition was 0.01 M $Zn(NO_3)_2$ and 0.1 M KCl, as well as current value was -0.3 mA cm^{-2}. During the synthesis, the potential value remains constant at about -1.1 V (vs. Ag/AgCl) that demonstrates deposition of ZnO particles, consistently.

Mechanism of ZnO deposition is summarized with the reactions given in equations 11-13, in aqueous $Zn(NO_3)_2$ solution [7]. In the first stage, reduction of NO_3^- anions yields OH^- anions at interface of electrode/solution. Afterward, the produced OH^- anions get together with Zn^{2+} cations at once, thus the production of $Zn(OH)_2$ takes place on the surface, that is hydroxylation process. Finally, $Zn(OH)_2$ gives the ZnO under the temperature, namely dehydration process.

$$NO_{3(aq)}^- + H_2O_{(l)} + 2e \rightarrow NO_{2(aq)}^- + 2\,OH_{(aq)}^- \quad (11)$$

$$Zn^{2+}_{(aq)} + 2\,OH_{(aq)}^- \rightarrow Zn(OH)_{2(s)} \quad (12)$$

$$Zn(OH)_{2(s)} \rightarrow ZnO_{(s)} + H_2O_{(l)} \quad (13)$$

3.7. Surface Morphology of CdSe/ZnO Nanorods

FE-SEM images were represented for ZnO nanostructures deposited on ITO/CdSe surface, in Figure 6b. It was proven that the deposited ZnO layer was comprised of rod-shaped particles, with various diameters. The formation of a dense structure on the surface is related to applied current value for 30 min deposition time. The polar crystal structure of ZnO consists of terminated positively Zn^{2+} (0001), as well as terminated negatively O^{2-} (000$\bar{1}$) polar planes. Thus, there is a net dipole moment throughout c-axis. Growth of ZnO oriented (0001) polar plane will be faster due to higher surface energy of (0001) polar surface than the other non-polar surfaces. Moreover, coulombic interaction between negatively charged ions and positive (0001) polar plane gives preferential growth for ZnO alongside c-axis [35,36]. Besides, the growth position of every nanostructure will affect the alignment of newly growing others in the neighborhood.
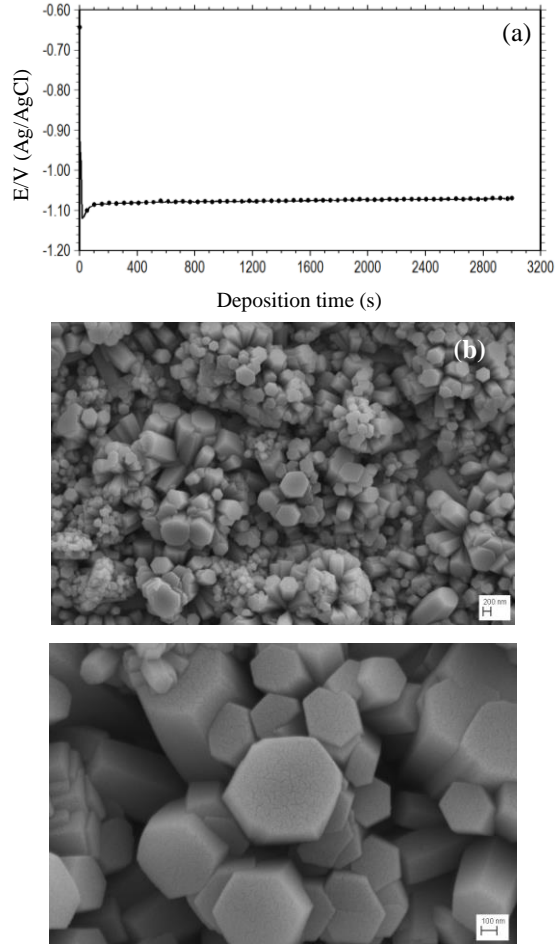

Figure 6. The chronopotentiogram plot during the deposition of ZnO nanostructures on ITO/CdSe (a) and FE-SEM images of CdSe/ZnO nanorods at different magnitudes (b)

3.8. Structural Property of CdSe/ZnO Nanorods

XRD pattern of CdSe/ZnO material was given in Figure 7a. XRD outcomes revealed ZnO nanorods are hexagonal wurtzite structure. The characteristic diffraction peaks detected at 2θ= 31.96°, 34.39°, 36.45°, 47.48° and 56.75° were connected to (100), (002), (101), (102) and (110) crystal surface of hexagonal wurtzite ZnO, respectively. This result is consistent with literature (PDF card no: 36-1451) [37].

Furthermore, diffraction peaks were obtained related to (111) and (220) crystalline surface of CdSe in CdSe/ZnO material. Furthermore, due to the thicker ZnO nanorods on the surface of ITO/CdSe, the peaks of ZnO hexagonal wurtzite crystal structure were more dominant. Besides, the density of peak related to (002) plane of ZnO nanostructures was stronger than the others, indicating that favored growing of ZnO nanorods were alongside the c-axis.

The volume of unit cell and lattice constant (a and c) were determined for ZnO by the following equations [38], where d is interplanar spacing of atomic planes. Also, (hkl) is the Miller indices of lattice constant. Moreover, lattice parameters

(c and a=b) of hexagonal rod-like ZnO were determined as 5.2376 Å and 3.2301 Å, respectively. The obtained values are consistent with standard values (c= 5.2066 Å and a= 3.2498 Å). The values of V and average D were also calculated as 47.32 Å^3 and 20.7254 nm, respectively for ZnO in CdSe/ZnO heterostructure.

$$\frac{1}{d_{hkl}^2} = \frac{4}{3}\left(\frac{h^2 + hk + k^2}{a^2}\right) + \frac{l^2}{c^2} \tag{14}$$
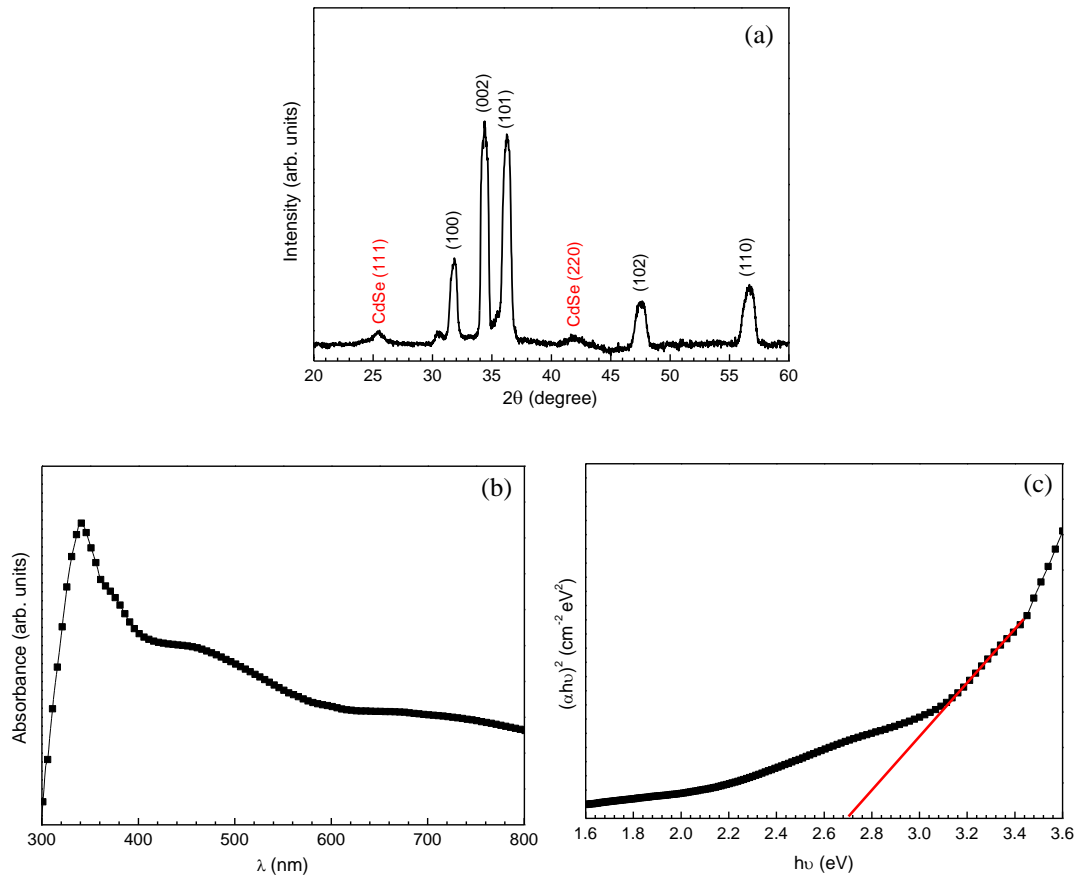
$$V = 0.866\, a^2\, c \tag{15}$$

Figure 7. XRD pattern of CdSe/ZnO nanorods (a) and absorbance (b) and Tauc plots of CdSe/ZnO nanorods (c)

3.9. Optical Property of CdSe/ZnO Nanorods

The optical behavior of CdSe/ZnO bilayer film was examined with help UV-visible studies. Absorbance spectrum of heterostructure material was given in Figure 7b. Furthermore, Tauc equation was utilized for determination of the band gap energy value, which was 2.7 eV (Figure 7c). The presence of ZnO particles on the top increased the band gap value with respect to single CdSe layer (2.0 eV). Absorption ability of narrow band gap semiconductors increases towards visible region compared to wide band gap semiconductors. Nevertheless, semiconductors with narrow band gap display lower photo catalytic efficiency because of rapid recombination rate of photo generated e/h$^+$ pairs [14]. In that context, prepared CdSe/ZnO material is said to have effective absorption capability in visible area of solar spectra. In the literature, similar results were given for various heterostructures [14,16]. The band gap value of the electrochemically prepared ZnO/CdS material was determined as 2.25 eV, which was 3.25 eV for solely ZnO [39]. As a conclusion, this kind of bilayer structures offer high catalytic efficiency with decreased band gap value and high stability.

3.10. The Electronic Parameters of CdSe and CdSe/ZnO Nanorods

Mott-Schottky analysis offers significant information regarding the electronic features of semiconductor material. For n type semiconductor, Mott-Schottky equation is given as below [40], where ε and ε_0 are relative permittivity of ZnO and CdSe (ε= 10 and 10.2). C is interfacial capacitance (F cm^{-2}) while vacuum permittivity is 8.854×10^{-12} F m^{-1}, respectively. E_{FB} and N_D are the values of flat band potential and charge carrier density, respectively. Furthermore, e is elementary electric charge (1.602×10^{-19} C) and E is applied potential (V).

$$\frac{1}{C^2} = \frac{2}{e\varepsilon\varepsilon_0 N_D}\left[\left(E-E_{FB}\right)-\frac{kT}{e}\right] \qquad (16)$$

Mott-Schottky graphs for CdSe and CdSe/ZnO materials were given in Figure 8. N_D values were calculated from slope of linear section As Mott-Schottky plots exhibit positive slope for CdSe and CdSe/ZnO, they are both n type semiconductors as given in Figure 8. E_{FB} values were determined with extrapolating in straight line to intersect x-axis. The depletion layer becomes positively charged while potential of semiconductor/solution interface shifts to positive potentials. Therefore, hole density increases at the surface, this provides inductive influence on solution side that produces charge deposition at interfacial area. Consequently, corresponding capacitance value and the slope of Mott-Schottky plot are due to change, as a function of potential.
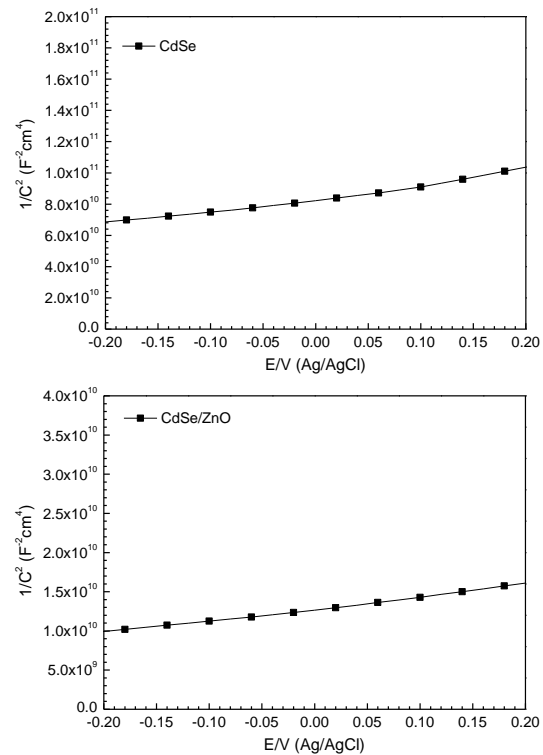

Figure 8. Mott-Schottky plots for CdSe and CdSe/ZnO materials

N_D values were found to be 1.623×10^{20} and 9.186×10^{20} cm^{-3} for CdSe and CdSe/ZnO, respectively. Also, E_{FB} values were found to be -0.981 V and -0.834 V for CdSe and CdSe/ZnO,

respectively. E_{FB} values of CdSe/ZnO electrode shifted to more positive values, with respect to CdSe. This situation is related to E_{FB} value of ZnO which is much more positive than CdSe [41]. Besides, more negative values of E_{FB} for n type semiconductor is related to effective charge transfer process, namely lower recombination rate for electron/hole pairs [42]. Therefore, mobility of charge carriers at interface of semiconductor/ solution was improved. N_D value of bilayered CdSe/ZnO nanostructure is almost ten times higher than CdSe. As a result, increasing the charge carrier density has a significant effect on higher photo catalytic performance of the material.

4. CONCLUSIONS

From cyclic voltammetry studies, it was shown that CdSe thin films could be deposited, under - 0.70 V (vs. Ag/AgCl) constant potential condition from aqueous solution of Cd^{2+} and Se^{4+}, in presence of Na_2SO_4 supporting electrolyte. The deposition time was important for the morphology, optical and electronic properties. FE-SEM results depicted that similar size (less than 10 nm) and shape CdSe particles are formed homogenously on the surface, and the particle size increases with increasing deposition time. EDX results revealed that the deposited films have almost the atomic ratio of 1:1 (Cd:Se), except 20 minutes deposition result. This was related to higher amount of selenium ions existing at the ITO electrode/solution interface, rather than cadmium ions which should be transported from bulk solution. XRD patterns represented that CdSe nanostructures were crystallized in cubic crystal structure. It was seen that from E_g values determined from Tauc plot were close to each other. The E_g values were in the range of 1.88 and 2.0 eV for CdSe thin films. Furthermore, ZnO nanorods were electrodeposited successfully on CdSe nanoparticles. The band gap value of CdSe/ZnO nanonorods was calculated as 2.7 eV. Flat band potentials of the CdSe and CdSe/ZnO materials were found as -0.981 V and -0.834 V, respectively. Besides, N_D values were determined as 1.623×10^{20} and 9.186×10^{20} cm^{-3} for CdSe and CdSe/ZnO, respectively. As a result, all findings demonstrated that homogenous well-defined and crystallized CdSe and CdSe/ZnO nanostructures were synthesized via electrochemical deposition method. ZnO top layer offers higher stability and low band gap (with respect to ZnO) is promising for such heterostructure material to be used in solar cell applications.

5. ACKNOWLEDGEMENTS

6. REFERENCES

1. Pulipaka, S., Boni, N., Ummethala, G., Meduri, P., 2020. CuO/CuBi$_2$O$_4$ Heterojunction Photocathode: High Stability and Current Densities for Solar Water Splitting. J. Catal., 387, 17-27

2. Yadav, A.A., Barote, M.A, Masumdar, E.U., 2010. Photoelectrochemical Properties of Spray Deposited n-CdSe Thin Films. Sol. Energy, 84, 763-770.

3. Choudhary, S., Upadhyay, S., Kumar, P., Singh, N., Satsangi, V.R., Shrivastav, R., Dass, S., 2012. Nanostructured Bilayered Thin Films in Photoelectrochemical Water Splitting-A Review. Int. J. Hydrogen Energy, 37, 18713-18730.

4. Mu, J., Teng, F., Miao, H., Wang, Y., Hu, X., 2020. In-situ Oxidation Fabrication of 0D/2D SnO$_2$/SnS$_2$ Novel Step-scheme Heterojunctions with Enhanced Photoelectrochemical Activity for Water Splitting. Appl. Surf. Sci., 501, 143974.

5. Qiu, Y., Pan, Z., Chen, H., Ye, D., Guo, L., Fan, Z., Yang, S., 2019. Current Progress in Developing Metal Oxide Nanoarrays-based Photoanodes for Photoelectrochemical Water Splitting. Sci. Bull., 64, 1348-1380.

6. Ma, H.P., Yang, J.H., Tao, J.J., Yuan, K.P., Cheng, P.H., Huang, W., Wang, J.C., Guo, Q.X., Lu, H.L., Zhang, D.W., 2019. Low-temperature Epitaxial Growth of High-quality

GaON Films on ZnO Nanowires for Superior Photoelectrochemical Water Splitting. Nano Energy, 66, 104089.

7. Sun, S., Jiaon, S., Zhang, K., Wang, D., Gao, S., Li, H., Wang, J., Yu, Q., Guo, F., Zhao, L., 2012. Nucleation Effect and Growth Mechanism of ZnO Nanostructures by Electrodeposition from Aqueous Zinc Nitrate Baths. J. Cryst. Growth, 359, 15-19.

8. Lianos, P., 2011. Production of Electricity and Hydrogen by Photocatalytic Degradation of Organic Wastes in a Photoelectrochemical Cell The Concept of the Photofuelcell: A Review of a Re-emerging Research Field. J. Hazard. Mater., 185, 575-590.

9. Jie, J., Zhang, W., Bello, I., Lee, C.S., Lee, S.T., 2010. One-dimensional II-VI Nanostructures: Synthesis, Properties and Optoelectronic Applications. Nano Today, 5, 313-336.

10. Gudade, Y.G., Deshpande, N.G., Sagade, A.A., Sharma, R.P., Pawar, S.M., Bhosale, C.H., 2007. Photoelectrochemical (PEC) Studies on CdSe Thin Films Electrodeposited from Non-aqueous Bath on Different Substrates. Bull. Mater. Sci., 30, 321-327.

11. Gholami Hatam, E., Ghobadi, N., 2016. Effect of Deposition Temperature on Structural, Optical Properties and Configuration of CdSe Nanocrystalline Thin Films Deposited by Chemical Bath Deposition. Mater. Sci. Semicond. Process., 43, 177-181.

12. Mariappan, R., Ponnuswamy, V., Mohan, S.M., Suresh, P., Suresh, R., 2012. The Effect of Potential on Electrodeposited CdSe Thin Films. Mater. Sci. Semicond. Process., 15, 174-180.

13. Thanikaikarasan, S., Sundaram, K., Mahalingam, T., Velumani, S., Rhee, J.K., 2010. Electrodeposition and Characterization of Fe Doped CdSe Thin Films from Aqueous Solution. Mater. Sci. Eng., B, 174, 242-248.

14. Wei, S., Chen, Y., Ma, Y., Shao, Z., 2010. Fabrication of CuO/ZnO Composite Films with Cathodic Co-electrodeposition and Their Photocatalytic Performance. J. Mol. Catal. A: Chem., 331, 112-116.

15. Dhara, A., Show, B., Baral, A., Chabri, S., Sinha, A., Bandyopadhyay, N.R., Mukherjee, N., 2016. Core-shell CuO-ZnO p-n Heterojunction with High Specific Surface Area for Enhanced Photoelectrochemical (PEC) Energy Conversion. Sol. Energy, 136, 327-332.

16. Wei, S., Shao, Z., Lu, X., Liu, Y., Cao, L., He, Y., 2009. Photocatalytic Degradation of Methyl orange over ITO/CdS/ZnO Interface Composite Films. J. Environ. Sci., 21, 991-996.

17. Lupan, O., Pauporte, T., Chow, L., Viana, B., Pelle, F., Ono, L.K., Roldan, Cuenya, B., Heinrich, H., 2010. Effects of Annealing on Properties of ZnO Thin Films Prepared by Electrochemical Deposition in Chloride Medium. Appl. Surf. Sci., 256, 1895-1907.

18. Sığırcık, G., 2017. Ni Katkılı ZnO, CdSe ve CdSe/ZnO Fotoaktif Malzeme Geliştirilmesi. Doktora Tezi, Çukurova Üniversitesi, Fen Bilimleri Enstitüsü, Kimya Anabilim Dalı, Adana, 129.

19. Lai, E., Kim, W., Yang, P., 2008. Vertical Nanowire Array-based Light Emitting Diodes. Nano Res., 1, 123-128.

20. Fang, J., Fan, H., Tian, H., Dong, G., 2015. Morphology Control of ZnO Nanostructures for High Efficient Dye-sensitized Solar Cells. Mater. Charact., 108, 51-57.

21. Bai, S., Sun, C., Guo, T., Luo, R., Lin, Y., Chen, A., Sun, L., Zhang, J., 2013. Low Temperature Electrochemical Deposition of Nanoporous ZnO Thin Films as Novel NO_2 Sensors. Electrochim. Acta, 90, 530-534.

22. Liu, Z., Bai, H., Xu, S., Delai, Sun, D., 2011. Hierarchical CuO/ZnO "Corn-like" Architecture for Photocatalytic Hydrogen Generation. Int. J. Hydrogen Energy, 36, 13473-13480.

23. Lin, Y., Yang, J., Zhou, X., 2011. Controlled Synthesis of Oriented ZnO Nanorod Arrays by Seed-layer-free Electrochemical Deposition. Appl. Surf. Sci., 258, 1491-1494.

24. Nikam, P.R., Baviskar, P.K., Sali, J.V., Gurav, K.V., Kim, J.H., Sankapal, B.R., 2015. SILAR Coated Bi_2S_3 Nanoparticles on Vertically Aligned ZnO Nanorods: Synthesis and Characterizations. Ceram. Int., 41, 10394-10399.

25. Pourbaix, M., 1974. Atlas of Electrochemical Equilibria in Aqueous Solution. Second Edition. NACE Pub., Houston.

26. Kois, J., Bereznev, S., Volobujeva, O., Gurevits, J., Mellikov, E., 2011. Electrocrystallization of CdSe from Aqueous Electrolytes: Structural Arrangement from Thin Films to Self-assembled Nanowires. J. Cryst. Growth, 320, 9-12.

27. Bienkowski, K., Strawski, M., Maranowski, B., Szklarczyk, M., 2010. Studies of Stoichiometry of Electrochemically Grown CdSe Deposits. Electrochim. Acta, 55, 8908-8915.

28. Powder Diffraction File 00-019-0191, International Center for Diffraction Data.

29. Klug, H.P., Alexander, L.E., 1974. X-ray Diffraction Procedures for Polycrystalline and Amorphous Materials. 2nd Edition, Wiley, New York.

30. Dhanam, M., Prabhu, R.R., Manoj, P.K., 2008. Investigations on Chemical Bath Deposited Cadmium Selenide Thin Films. Mater. Chem. Phys., 107, 289-296.

31. Aragonès, A.C., Palacios-Padrós, A., Caballero-Briones F., Sanz F., 2013. Study and Improvement of Aluminium Doped ZnO Thin Films: Limits and Advantages. Electrochim. Acta, 109, 117-124.

32. Shyju, T.S., Anandhi, S., Indirajith, R., Gopalakrishnan, R., 2011. Solvothermal Synthesis, Deposition and Characterization of Cadmium Selenide (CdSe) Thin Films by Thermal Evaporation Technique. J. Cryst. Growth, 337, 38-45.

33. Pawar, S.A., Patil, D.S., Suryawanshi, M.P., Ghorpade, U.V., Lokhande, A.C., Park, J.Y., Chalapathy R.B.V., Shin J.C., Patil P.S., Kim J.H., 2016. Effect of Different Annealing Environments on the Solar Cell Performance of CdSe Pebbles. Acta Mater., 108, 152-160.

34. Zhao, Y., Yan, Z., Liu, J., Wei, A., 2013. Synthesis and Characterization of CdSe Nanocrystalline Thin Films Deposited by Chemical Bath Deposition. Mater. Sci. Semicond. Process., 16, 1592-1598.

35. Zi, M., Zhu, M., Chen, L., Wei, H., Yang, X., Cao, B., 2014. ZnO Photoanodes with Different Morphologies Grown by Electrochemical Deposition and their Dye-Sensitized Solar Cell Properties. Ceram. Int., 40, 7965-7970.

36. Xue, B., Liang, Y., Donglai, L., Eryong, N., Congli, S., Huanhuan, F., Jingjing, X., Yong, J., Zhifeng J., Xiaosong S., 2011. Electrodeposition from ZnO Nano-rods to Nano-sheets with only Zinc Nitrate Electrolyte and its Photoluminescence. Appl. Surf. Sci., 257, 10317-10321.

37. Powder Diffraction File 00-036-1451, International Center for Diffraction Data.

38. Cullity, B.D. and Stock, S.R., 2001. Elements of X-Ray Diffraction. 3rd Edition, Prentice Hall Inc., New Jersey.

39. Li, H., Yao, C., Meng, L., Sun, H., Huang, J., Gong Q., 2013. Photoelectrochemical Performance of Hydrogenated ZnO/CdS Core-Shell Nanorod Arrays. Electrochim. Acta, 108, 45-50.

40. Ahn, K.S., Deutsch, T., Yan, Y., Jiang, C.S., Perkins, C.L., Turner, J., Al-Jassim, M., 2007. Synthesis of Band-gap-reduced p-type ZnO Films by Cu Incorporation. J. Appl. Phys., 102:023517, 1-6.

41. Liu, H., Piret, G., Sieber, B., Laureyns, J., Roussel, P., Xu, W., Boukherrou, R., Szunerits, S., 2009. Electrochemical Impedance Spectroscopy of ZnO Nanostructures. Electrochem. Commun., 11, 945-949.

42. Rokade, A., Rondiya, S., Sharma, V., Prasad, M., Pathan, H., Jadkar, S., 2017. Electrochemical Synthesis of 1D ZnO Nanoarchitectures and their Role in Efficient Photoelectrochemical Splitting of Water. J. Solid State Electrochem., 21, 2639-2648.